JACS
JOURNAL OF THE AMERICAN CHEMICAL SOCIETY

Article

pubs.acs.org/JACS

Direct Quantification of Loop Interaction and $\pi-\pi$ Stacking for G-Quadruplex Stability at the Submolecular Level

Chiran Ghimire,[†] Soyoung Park,[‡,§] Keisuke Iida,[∥] Philip Yangyuoru,[†] Haruka Otomo,[‡,§] Zhongbo Yu,[†] Kazuo Nagasawa,*[,∥] Hiroshi Sugiyama,*[,‡,§] and Hanbin Mao*[,†]

[†]Department of Chemistry and Biochemistry and School of Biomedical Sciences, Kent State University, Kent, Ohio 44242, United States

[‡]Department of Chemistry, Graduate School of Science, Kyoto University, Kitashirakawa-oiwakecho, Sakyo-ku, Kyoto 606-8502, Japan

[§]Institute for Integrated Cell Material Sciences (iCeMS), Kyoto University, Yoshida-ushinomiyacho, Sakyo-ku, Kyoto 606-8501, Japan

[∥]Department of Biotechnology and Life Science Faculty of Technology, Tokyo University of Agriculture and Technology (TUAT), Koganei, Tokyo 184-8588, Japan

Supporting Information

ABSTRACT: The well-demonstrated biological functions of DNA G-quadruplex inside cells call for small molecules that can modulate these activities by interacting with G-quadruplexes. However, the paucity of the understanding of the G-quadruplex stability contributed from submolecular elements, such as loops and tetraguanine (G) planes (or G-quartets), has hindered the development of small-molecule binders. Assisted by click chemistry, herein, we attached pulling handles via two modified guanines in each of the three G-quartets in human telomeric G-quadruplex. Mechanical unfolding using these handles revealed that the loop interaction contributed more to the G-quadruplex stability than the stacking of G-quartets. This result was further confirmed by the binding of stacking ligands, such as telomestatin derivatives, which led to similar mechanical stability for all three G-quartets by significant reduction of loop interactions for the top and bottom G-quartets. The direct comparison of loop interaction and G-quartet stacking in G-quadruplex provides unprecedented insights for the design of more efficient G-quadruplex-interacting molecules. Compared to traditional experiments, in which mutations are employed to elucidate the roles of specific residues in a biological molecule, our submolecular dissection offers a complementary approach to evaluate individual domains inside a molecule with fewer disturbances to the native structure.

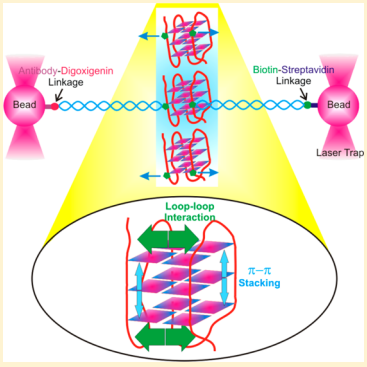

INTRODUCTION

With firm demonstration of in vivo formation of DNA G-quadruplexes,[1] research focus in the field has now shifted to their biological functions. It has been shown that G-quadruplex formed in the single-stranded telomeric region can inhibit telomerase, an enzyme overexpressed in 80% of cancer cells to elongate telomere overhang, which leads to cell immortality.[2,3] The inhibition of telomerase can be tuned by G-quadruplex-binding ligands, such as telomestatin.[4] Due to potential pharmaceutical applications, this finding has attracted an intensive research interest. As a motor protein, telomerase can be stopped by a roadblock whose mechanical stability is higher than the stall force of the enzyme.[5] Elucidation of the mechanical property of the G-quadruplex/ligand complex is therefore instrumental to design more effective molecules that can strengthen G-quadruplex as a mechanical blocker not only to telomerase but also to other motor proteins, such as RNA and DNA polymerases.

G-quadruplex has a rather unique topology.[6] It is composed of a stack of G-quartet planes, each of which is joined by four guanine residues through Hoogsteen base pairs (Figure 1a, inset). It has been generally accepted that the stacking between G-quartets provides stability to a G-quadruplex, whereas the size and the orientation of the loops determine the type and the flexibility of the structure.[7] The importance of the G-quartet stacking to the structural stability has been supported by the binding geometry of many ligands that stack onto G-quartet planes.[8] Recent findings, however, have suggested that the loop interaction is also important for the structural stability.[9,10] Due to the lack of appropriate techniques, however, the relative contribution of G-quartet stacking and loop interaction to the G-quadruplex stability has not been resolved unambiguously. We reasoned that by submolecular dissection of a G-quadruplex in a quartet-by-quartet fashion, we may directly distinguish the contribution of the G-quartet stacking and loop interaction to the stability of G-quadruplex.

Received: April 10, 2014
Published: October 8, 2014

dx.doi.org/10.1021/ja503585h | J. Am. Chem. Soc. 2014, 136, 15537−15544

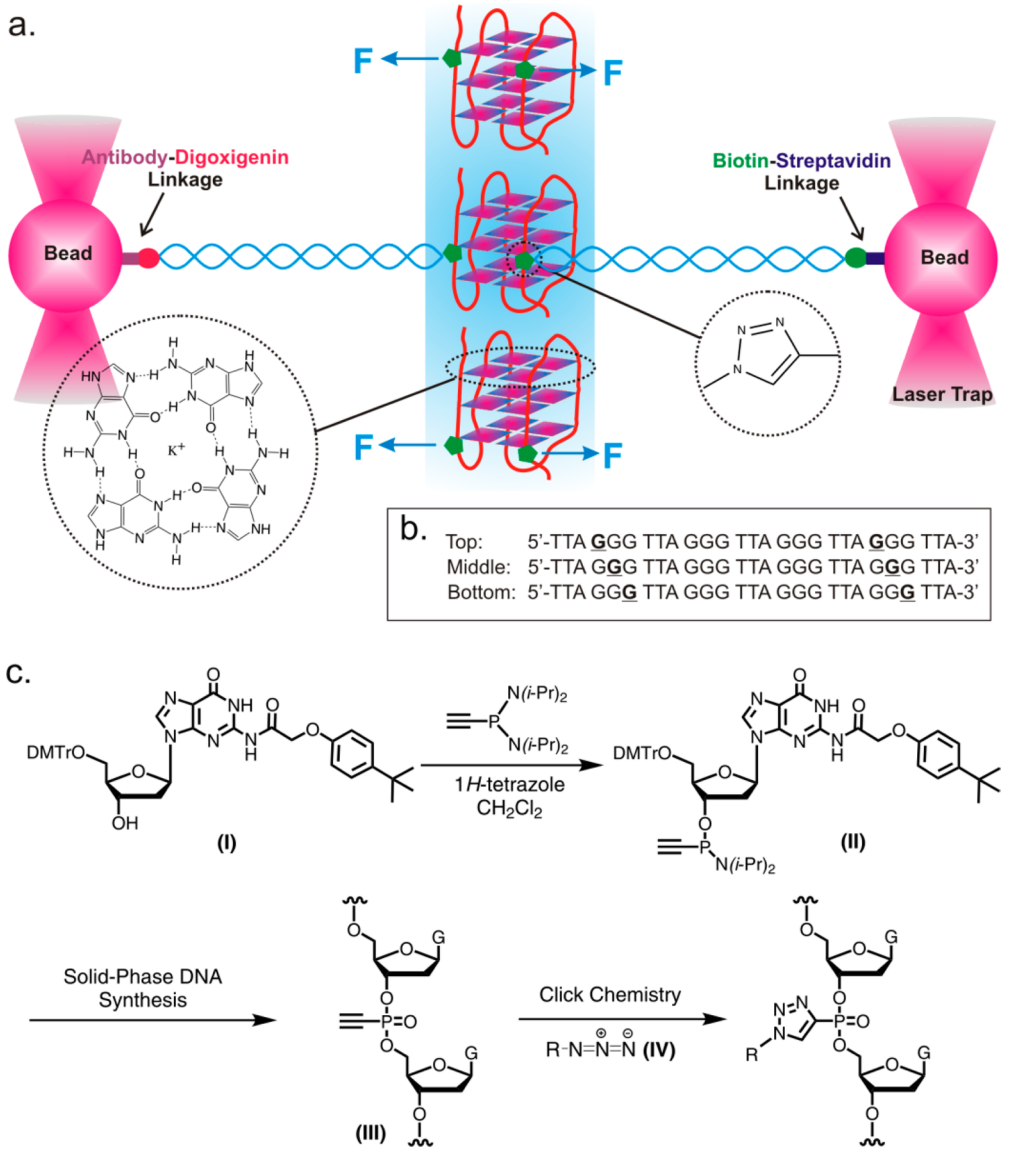

Figure 1. Dissection of DNA structures at the submolecular level. (a) Experimental setup for the quartet-by-quartet dissection of G-quadruplex. A G-quartet structure and a click chemistry linkage (triazole) are shown in the left and right insets, respectively. (b) Human telomeric sequences with alkyne-modified guanine residues (underlined) in the top, middle, or bottom G-quartet of an expected hybrid-1 G-quadruplex. (c) Synthesis of alkyne-modified telomeric sequences. An alkyne-modified guanine residue for solid-phase synthesis (**II**) was prepared from compound **I**. After incorporation of **II** into oligodeoxynucleotides (**III**) via solid-phase synthesis, a dsDNA handle terminated with an azide group (**IV**) was attached to **III** through click chemistry (see Materials and Methods for details).

Previously, we have probed the mechanical property of DNA G-quadruplexes with and without ligands using optical tweezers.[11,12] Assisted by click chemistry,[13] we have been able to attach pulling handles to one or two loops, from which the unfolding and refolding of telomeric G-quadruplex can be investigated along specific geometries. To dissect a G-quadruplex quartet-by-quartet, pulling handles are designed to attach to the 3′-phosphate of the particular pair of guanine residues in the top, middle, or bottom G-quartet separately (Figure 1c). The mechanical unfolding experiments via these pulling handles revealed that unfolding forces of the overall G-quadruplex are smaller than those through loops, suggesting that loops contribute more to the structural stability than the G-quartets. Among the three G-quartets in a telomeric G-quadruplex, the middle quartet presents the weakest mechanical stability. This is consistent with the least interaction between the loops and the middle G-quartet, confirming that the quartet stacking is weaker than the loop interaction. Binding of telomestatin derivatives corroborates this finding. When a telomestatin dimer binds to G-quadruplex by stacking on both the top and bottom G-quartets, it leads to similar mechanical stabilities for all three G-quartets, probably due to the prevention of loop−quartet interactions. Whereas a telomestatin monomer and dimer demonstrate different mechanical stabilities for the bottom G-quartet, they share the same stability for the top G-quartet. This result is consistent with the NMR structure in which the monomer ligand prefers to stack on the top G-quartet. The submolecular dissection method, therefore, can be used conveniently to probe the ligand binding sites of biological molecules.

dx.doi.org/10.1021/ja503585h | J. Am. Chem. Soc. 2014, 136, 15537−15544

MATERIALS AND METHODS

Materials. Enzymes and plasmids were purchased from New England Bioabs (NEB). Nucleotides were purchased from Integrated DNA Technology (IDT). Polystyrene beads coated with streptavidin or anti-digoxigenin antibody were purchased from Spherotech (Lake Forest, IL). All other chemicals (>99% purity, unless specified) were purchased from VWR.

Synthesis of 5′-*O*-Dimethoxytrityl-N^2-*tert*-butylphenoxyacetyl-2′-deoxyriboguanosine 3′-*O*-Ethynylphosphinoamidite. Bis(*N*,*N*-diisopropylamino)ethynylphosphine (compound **II** in Figure 1c) was prepared by Grignard reaction using bis(*N*,*N*-diisopropylamino)chlorophosphine and ethynylmagnesium bromide as reported previously.[14] The solution of 5′-DMT-N^2-*tert*-butylphenoxyacetyl-2′-deoxyguanosine (0.82 mmol, 1.0 equiv, compound **I** in Figure 1c) and 1*H*-tetrazole was prepared in anhydrous dichloromethane (10 mL) under argon. Bis(*N*,*N*-diisopropylamino)-ethynylphosphine (1.64 mmol, 2.0 equiv) in anhydrous dichloromethane (20 mL) was placed in a 100 mL two-neck round-bottom flask with a 50 mL addition funnel. To a solution of bis(*N*,*N*-diisopropylamino)ethynylphosphine was dropwise added 2′-deoxyriboguanosine and 1*H*-tetrazole in dichloromethane over 15 min and the mixture stirred for 30 min at room temperature under argon. After completion of the reaction, triethylamine was added to neutralize the reaction mixture and the solvent was removed in a vacuum. The residue was purified by column chromatography using a 50−100% gradient of ethyl acetate in hexane containing 1% triethylamine to afford an amorphous, ivory solid (341 mg, 45% yield). ^{31}P NMR ($CDCl_3$): δ 97.2, 96.0. ^{1}H NMR ($CDCl_3$): δ 7.83 (d, $^4J_{HH}$ = 1.4 Hz, 1H), 7.41−7.37 (m, 4H), 7.30−7.24 (m, 7H), 7.19 (td, $^3J_{HH}$ = 7.1 Hz and $^4J_{HH}$ = 1.4 Hz, 1H), 6.92 (d, $^3J_{HH}$ = 8.9 Hz, 2H), 6.79 (dd, $^3J_{HH}$ = 5.8 Hz and $^4J_{HH}$ = 2.7 Hz, 4H), 6.32 (ddd, $^2J_{HH}$ = 13.6 Hz, $^3J_{HH}$ = 6.1 Hz and $^4J_{HH}$ = 1.3 Hz, 1H), 4.70−4.66 (m, 1H), 4.64−4.63 (m, 2H), 4.30−4.26 (m, 1H), 3.77 (s, 6H), 3.37−3.28 (m, 2H), 3.07 (dd, $^3J_{HH}$ = 11.9 Hz and $^4J_{HH}$ = 1.7 Hz, 1H), 2.66−2.53 (m, 2H), 1.32 (s, 9H), 1.19−1.17 (m, 9H), 1.12 (t, $^3J_{HH}$ = 6.8 Hz, 3H). ^{13}C NMR ($CDCl_3$): δ 169.9, 158.8, 155.6, 154.4, 147.9, 146.3, 146.2, 144.6, 137.2, 135.8, 130.2, 128.3, 128.1, 127.1, 127.0, 122.3, 114.6, 113.4, 92.3, 86.8, 86.3, 86.1, 85.6, 83.9, 76.4, 67.4, 63.7, 55.4, 34.5, 31.6, 24.5. HRMS (ESI): calcd for $C_{51}H_{59}N_6NaO_8P$ $[M + Na]^+$ 937.4030, found 937.4024.

Oligodeoxynucleotide (ODN) Synthesis. ODNs (compound **III** in Figure 1c) were synthesized on solid supports using alkyne-modified phosphinoamidite and commercially available $O^{5'}$-dimethoxytrityl-2′-deoxyribonucleoside-$O^{3'}$-phosphoramidites. Solid-phase oligonucleotide synthesis was performed on an ABI DNA synthesizer (Applied Biosystem, Foster City, CA). The alkyne-modified phosphinoamidite was chemically synthesized as described above and incorporated without purification into oligonucleotide through coupling reactions for 10 min. Coupling yields with alkyne-modified phosphinoamidites were equal to the ones obtained with standard phosphoramidite building blocks. Cleavage from the solid support was performed with 50% of anhydrous ethylenediamine in toluene at room temperature for 2 h. The cleavage mixture was discarded and the solid-support was dried using a SpeedVac. The crude oligonucleotides were obtained by washing the support with 5% acetonitrile in water (1 mL) and purified by RP-HPLC using a linear gradient of 0 to 100% acetonitrile over 40 min at a flow rate 1.5 mL/min (50 mM TEAA solution was used). The trityl-on fractions were collected and dried using a SpeedVac. The deprotection of trityl group was carried out with an 80% acetic acid solution for 2 h. After a second purification by RP-HPLC, alkyne-modified oligonucleotide was collected by freeze-drying. DNA concentrations were determined by using the Nano drop ND-1000 (Nanodrop Technologies, Wilmington, DE).

Synthesis of DNA Constructs for Mechanical Unfolding Experiments. To mechanically unfold and refold structures formed in telomeric DNA, the ethynyl-modified ssDNA fragments [the G4-G22 (top), G5-G23 (middle), and G6-G24 (bottom) constructs] prepared above were sandwiched between the two dsDNA strands of 2028 bp length. These two 2028 bp dsDNA handles were prepared separately by PCR from a pBR322 plasmid using two sets of primers. One set of primers contains azide and biotin, while the other contains azide and digoxigenin at the 5′-ends. Two 2028 bp dsDNA handles were mixed with alkyne-modified G4-G22, G5-G23, or G6-G24 in equimolar ratio (0.5 μM) in 10 μL aqueous solution, followed by adding freshly prepared 3 μL of a solution that contains DMS/*t*-ButOH 3:1 v/v with 33 mM CuBr and 67 mM TBTA (tris[(1-benzyl-1*H*-1,2,3-triazol-4-yl)methyl]amine, Sigma).[14,15] The reaction mixture was incubated overnight in the absence of light. The CuBr was removed by addition of equimolar amounts of EDTA, followed by ethanol precipitation. As a result of cyclic addition via click chemistry,[13] the ssDNA sequence was sandwiched between the two dsDNA handles.

Synthesis of Telomestatin Derivatives. Synthesis and structural characterizations of the derivatives were performed according to the precedent report.[16] All derivatives were prepared as 10 mM stock solutions in dimethyl sulfoxide (DMSO). Further dilutions to working concentrations were performed using 10 mM Tris buffer (pH 7.4) with 100 mM KCl.

Surface Plasmon Resonance (SPR) Binding Assay. The 5′-biotin-AGGG(TTAGGG)$_3$-3′ telomere DNA sequence used in the SPR experiments was purchased from Sigma Genosis (HPLC grade). The SPR binding experiments were performed with Biacore T-200 (GE Healthcare). The binding experiments were carried out according to the report by Hurley and co-workers as follows.[17−19] The biotin-labeled DNA was bound to a streptavidin-coated sensor chip (Series S Sensor Chip SA). One flow cell was used to immobilize the DNA [400 resonance units (RU)], while a second cell was left blank as a control. The binding experiments were performed in the sterile, filtered, and degassed HEPES buffer [0.01 M HEPES (pH 7.4), 3 mM EDTA, and 0.05% surfactant P20 with 100 mM KCl]. For binding experiments, an experimental solution of L2H2-6OTD monomer and its dimer was prepared in the HEPES buffer by serial dilutions from stock solution (10 mM). The experimental solutions at concentrations from 7.8 to 62.5 nM were injected through the DNA and blank flow cells at a rate of 100 μL/min at 25 °C until a constant steady-state response was obtained (300 s, Figure S1, Supporting Information). Compound solution flow was then replaced by buffer flow, resulting in dissociation of the complex (350 s). To remove any remaining bound compound after the dissociation phase of the sensorgram, a low-pH glycine regeneration buffer was used (10 mM glycine at pH 2). The reference response from the blank cell was subtracted from the response of the sample flow cell to give an instrument response (RU) that is directly proportional to the amount of L2H2-6OTD monomer and its dimer bound to the immobilized DNA. Reference-subtracted sensorgrams for each concentration were analyzed using the kinetics 1:1 binding program using BIAevaluation software. The dissociation constant (K_D) between G4 ligands and telomeric G4 is defined according to $K_D = k_d/k_a$, where k_a and k_d represent the kinetic constants for association and dissociation, respectively (see Table S1 of the Supporting Information for values).

Circular Dichroism (CD). Five micromolar DNA samples were dissolved in 10 mM Tris buffer (pH 7.4) with 100 mM KCl with (100 nM) or without telomestatin derivatives for CD spectra. Each spectrum was collected with a JASCO-810 spectropolarimeter (Easton, MD) using a quartz cuvette with a 1 mm optical path length at room temperature. The average spectra of three scans over the wavelength range of 220−320 nm were acquired with a scan rate of 100 nm/min. The background signals from the buffer were subtracted from the spectra of DNA samples and smoothed using the Savitzky−Golay function.

Single Molecule Force Ramp Assay. Single molecule force ramping was performed with home-built dual-trap optical tweezers[20] at 23 °C in 10 mM Tris buffer containing 100 mM KCl at pH 7.4, with and without telomestatin derivatives. Two kinds of polystyrene beads coated either with streptavidin or digoxigenin antibody were separately trapped by laser tweezers in a microfluidic chamber. The antibody-coated bead was incubated with the DNA construct prior to the laser trapping. One of the traps was fixed while the other was controlled by a steerable mirror. The DNA was tethered between the two polystyrene beads through affinity interactions between digoxigenin antibody and biotin−streptavidin complexes. When the two beads were moved apart, the tension in the DNA tether increased, which was

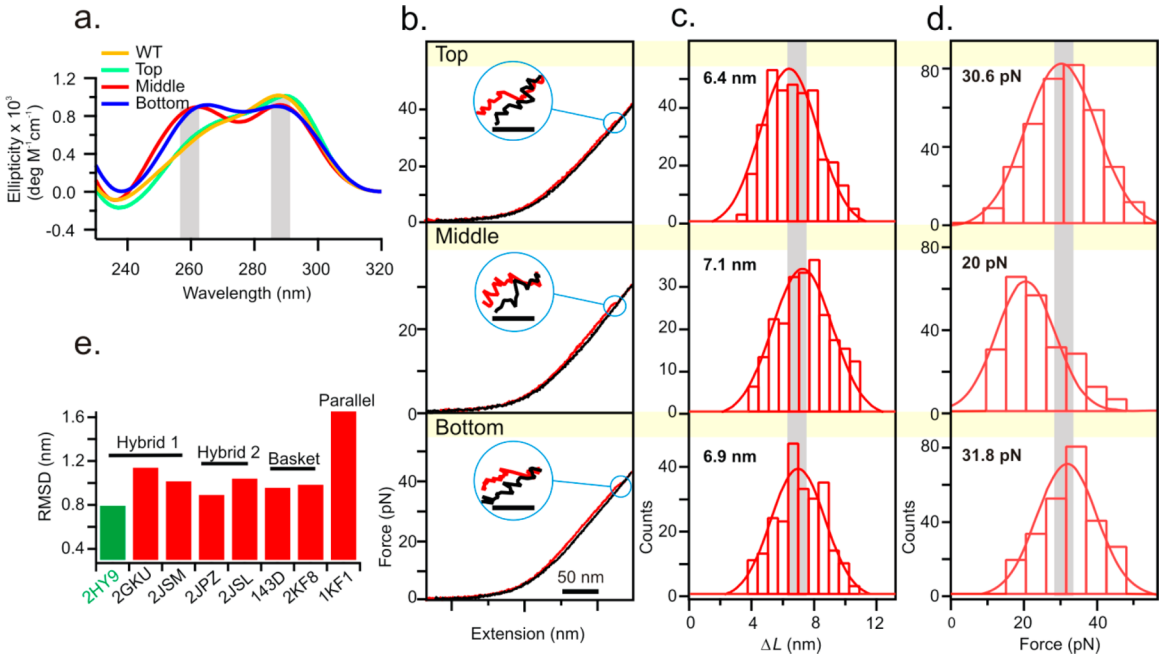

Figure 2. Mechanical unfolding of a hybrid-1 G-quadruplex. (a) Circular dichroism spectra of 5 μM wild type (WT) and the top, middle, and bottom telomeric sequences (see Figure 1b) in 10 mM Tris (pH 7.4) buffer with 100 mM KCl. (b–d) Single-molecule force ramp experiments for the top, middle, and bottom telomeric sequences in the same buffer. (b) Typical force–extension (F–X) curves. Scale bars in the blowup insert represent 10 nm. (c) Change in contour length (ΔL) of unfolded features. (d) Rupture force of unfolded features. (e) Root mean square difference (RMSD) of the appropriate inter-residue distances between known PDB structures and experimental measurements.

recorded in the force–extension (F–X) curves using the Labview program (National Instruments Corp., Austin, TX). We recorded the force range from 0 to 60 pN at 1000 Hz with a loading rate of 5.5 pN/s. The single molecular nature of the DNA was confirmed by the observation of the 65 pN plateau in the F–X curve.

The F–X curves were filtered using the Savitzky–Golay function with a time constant of 10 ms in the Matlab program (The Math Works, Nattick, MA). The change in extension (Δx) at a given force was calculated from the difference between stretching and relaxing curves at that force. The change in contour length (ΔL) was calculated from Δx using the wormlike chain model (WLC).[21]

$$\frac{\Delta x}{\Delta L} = 1 - \frac{1}{2}\sqrt{\frac{k_B T}{FP}} + \frac{F}{S}$$

where L is the contour length, k_B is the Boltzmann constant, T is the absolute temperature, P is the persistence length (50.8 nm),[22] and S is the stretching modulus (1243 pN).[22]

Wherever appropriate, three sets of experiments were performed to obtain standard deviations, which are reported in the main text or as error bars in figures.

Calculation of Change in the Free Energy of Unfolding. The change in free energy of unfolding a G-quadruplex (ΔG_{unfold}) was calculated using Jarzynski's equality equation under nonequilibrated conditions[23]

$$\Delta G_{unfold} = -k_B T \ ln \sum_{i=1}^{N} \frac{1}{N} \exp\left(-\frac{w_i}{k_B T}\right)$$

where N is the number of repetitions and w_i is the nonequilibrium work done to unfold the G-quadruplex. See the literature[11] for a detailed calculation of the work.

The bias for ΔG_{unfold} was estimated from the histogram of work distribution according to the literature.[24]

RESULTS AND DISCUSSION

Quartet-by-Quartet Dissection Suggests That Loop Interaction is a Predominant Factor for G-Quadruplex Stability.

The submolecular dissection of DNA G-quadruplex structure was carried out by laser tweezers, with which the mechanical unfolding of a biomacromolecule was carried out along specific trajectories defined by two residues that serve as pulling handles[15] (Figure 1a). To clearly differentiate different G-quartet layers, handle residues must be selected from the known G-quadruplex conformations. The human telomeric G-quadruplex structure can form a variety of different conformations dependent on solvent conditions or flanking sequences.[7] In our previous investigations, we have determined that hybrid-1 G-quadruplex is the most likely conformation formed in the same sequence used here under single-molecular conditions.[22] Assuming this conformation, we chose G4 and G22 to attach the pulling handles for the top G-quartet, G5 and G23 for the middle G-quartet, and G6 and G24 for the bottom G-quartet (Figure 1b). We modified these G-residues with terminal alkynes through phosphate groups,[14] which allow the attachment of double-stranded DNA as pulling handles via click chemistry (see Materials and Methods and Figure 1c). Since the distance between the modified phosphate and the 5′-end guanine base in a specific G-quartet is shorter than that between the same phosphate and the 3′-end guanine base in another G-quartet (see Figure S2 and Table S2 in the Supporting Information), the tension felt by the G-quadruplex likely propagates through the 5′-end guanine pairs. By choosing the specific guanine pairs discussed above, we are able to unfold desired G-quartets in the hybrid-1 G-quadruplex.

To probe the G-quadruplex structures after the modification, we performed CD experiments (Figure 2a). A valley at 240 nm and two peaks at 260 and 290 nm suggested that the hybrid-1 G-quadruplex conformation[25] is maintained for all three mutants. Further confirmation of the hybrid-1 structure came from the single-molecule structural identification method based on the end-to-end distance measurements[15,22] (see below).

dx.doi.org/10.1021/ja503585h | J. Am. Chem. Soc. 2014, 136, 15537–15544

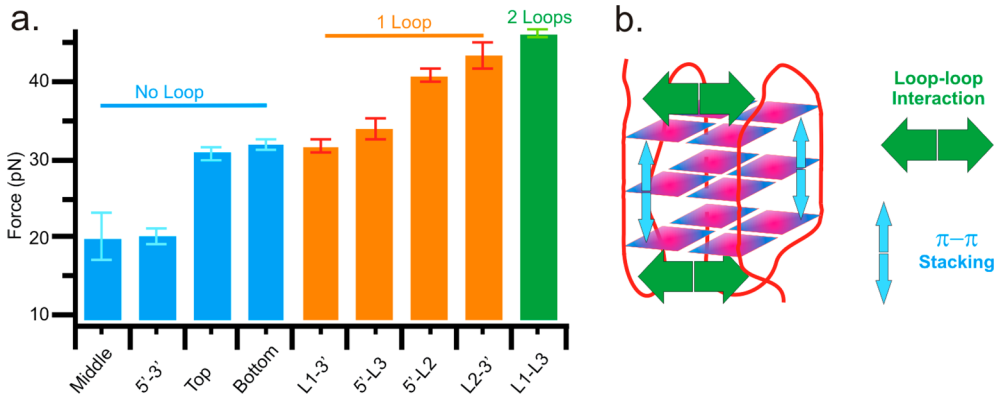

Figure 3. Loop interaction is stronger than the G-quartet stacking. (a) Rupture force for different unfolding geometries of human telomeric G-quadruplex. "Top", "middle", or "bottom" indicates unfolding through a particular G-quartet (see Figure 1a). "L1", "L2", and "L3" depict T9 in the first loop, T15 in the second loop, and T21 in the third loop, respectively, counted from the 5′-end of the G-quadruplex. The sequence of the G-quadruplex-forming sequence is 5′-T1T2A3G5G6G7**T8**T9A10G11G12G13**T14**T15A16G17G18G19**T20**T21A22G23G24G25T26T27A28-3′. (b) Schematic drawing depicts that the loop−loop interaction is stronger than the quartet stacking in a hybrid-1 telomeric G-quadruplex.

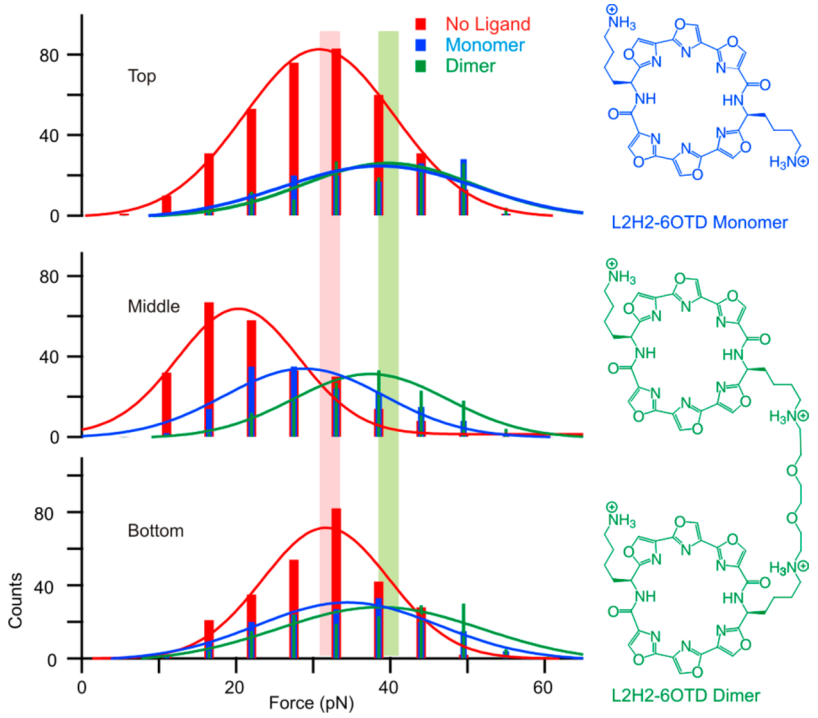

Figure 4. Effect of telomestatin derivatives on the stability of G-quadruplex. The left panel shows rupture force histograms from different G-quartets in the presence of either telomestatin monomer (blue) or dimer (green). Rupture force histograms of free G-quadruplexes are shown in red. The right panel depicts structures of telomestatin derivatives.

With this structural clarification, each set of the alkyne-modified telomeric sequences was reacted with two dsDNA handles labeled with azide at one of their ends through click chemistry[15] (see Materials and Methods). The attachment of the DNA constructs to two optically trapped polystyrene particles was achieved through the affinity linkage between the digoxigenin antibody and biotin−streptavidin complexes (Figure 1a). Using the single molecular force-ramp assay (see Materials and Methods), we observed rupture events that represent the unfolding of G-quadruplexes (Figure 2b). From each unfolding event, we measured the change in contour length (ΔL, Figure 2c) and the rupture force ($F_{rupture}$, Figure 2d), which depict the size and the mechanical stability of a G-quadruplex, respectively. The ΔL is in agreement with expected value of ∼6.6 nm from all three unfolding geometries (PDB code: 2HY9[25]). On the basis of these ΔL values, we calculated the end-to-end distance (x) between the two handle residues by the function $x = L - \Delta L$.[11] Here L is the contour length of the structure. After combining these distances with those between different pairs of residues measured previously,[15] we compared the corresponding distances obtained from the known human telomeric G-quadruplex structures. Evaluation using the RMSD (Figure 2e) between these two sets of data allowed us to conclude that the best matching conformation is the hybrid-1 G-quadruplex, therefore, confirming the CD results.

The $F_{rupture}$ histograms for the three G-quartets revealed (Figure 2d) that the rupture forces for the top and bottom G-quartets are similar, while that for the middle quartet is the

dx.doi.org/10.1021/ja503585h | J. Am. Chem. Soc. 2014, 136, 15537−15544

smallest. This result suggested that the loop interaction is a predominant factor for the stability of G-quadruplex. Since the top and the bottom quartets interact more extensively with the loops than the middle quartet, the rupture forces are higher for the top and the bottom G-quartets. When we summarized the rupture force for each pair of handle residues, we found that indeed, unfolding through loop residues has a higher rupture force than that through G-quartet residues (Figure 3a; see Table S3 of the Supporting Information for sequences). In fact, the highest rupture force is from the unfolding via two loop residues, T9 in loop1 and T21 in loop3. These results strongly supported that loop interactions have stronger mechanical stability than the stacking between G-quartets (Figure 3b). These loop interactions could have conceivably originated from hydrogen bonding between loop bases[26] and the stacking interaction of the bases in the loop and the G-quartet.[25,26]

Dissection of Telomestatin-Bound G-Quadruplex Confirmed That the Loop Interaction is Stronger Than the G-Quartet Stacking. To provide further evidence that the loop interaction is a predominant stabilization factor for human telomeric G-quadruplex, we proceeded to investigate the effect of ligand binding on the G-quadruplex stability. We chose telomestatin derivatives as model ligands, which are known to bind tightly with G-quadruplexes by stacking with terminal quartets.[4] NMR structures have revealed that a telomestatin monomer, L2H2-6OTD (Figure 4, blue), prefers to stack on the top G-quartet in a hybrid-1 telomeric G-quadruplex.[8] On the other hand, we designed an L2H2-6OTD dimer (Figure 4, green) with a flexible linker that matches with the height of the human telomeric G-quadruplex. This ligand is expected to stack on both the top and bottom G-quartets.[27,28] Due to this stacking, we reasoned that top or bottom G-quartet(s) may be shielded from loop interactions, which may result in similar rupture force as that for the middle G-quartet.

This scenario was exactly observed. To ensure the complete stacking of the dimer, we used a saturation concentration of 100 nM (K_D for the dimer is 8.3 nM; see Materials and Methods and Figure S1 and Table S1, Supporting Information). CD spectrum confirmed that the hybrid-1 G-quadruplex conformation is maintained after ligand binding (Figure S3b, Supporting Information). Comparison of the rupture forces revealed that they increase to the same value for all three G-quartets (38 ± 3, 37 ± 2, and 36.8 ± 0.4 pN for the top, middle, and bottom G-quartets, respectively, Figure 4), confirming that due to the stacking of the telomestatin dimer, the loops are shielded from interacting with both top and bottom G-quartets. The increased rupture force is a result of ligand binding, which stabilizes the G-quadruplex.[12] The stabilization has been corroborated by the measurement of the change in free energy of unfolding (ΔG_{unfold}) (Table 1; see Materials and Methods for calculations), which showed increased stability of G-quadruplex after binding with the telomestatin dimer (~14 vs ~9 kcal/mol for free G-quadruplex).

When we used 100 nM L2H2-6OTD monomer (K_D = 10.8 nM, Figure S1a and Table S1,Supporting Information), we found that G-quadruplex assumes the expected hybrid-1 conformation from CD signatures[8] (Figure S3a, Supporting Information). Comparison of the rupture force revealed that the top G-quartet (37 ± 1 pN) showed similar mechanical stability as that for the dimer binding (38 ± 3 pN, Figure 4 top). In contrast, the bottom G-quartet had a lower rupture force (34 ± 2 pN) than that bound with the dimer (36.8 ± 0.4 pN, Figure 4, bottom). This result is consistent with the fact that the L2H2-6OTD monomer prefers to bind to the top, instead of the bottom, G-quartet,[8] which reinforces the mechanical stability of the top G-quartet only. Similar to the dimer binding, the rupture forces for the monomer-bound structures are higher than for free G-quadruplexes along the same unfolding geometry, indicating again that ligand binding increases the overall stability of G-quadruplex.[12] The increased ΔG_{unfold} upon monomer binding (1−2 kcal/mol; see Table 1) confirmed this stability variation.

The overall ΔG_{unfold} trend (Table 1) revealed that G-quadruplex bound with telomestatin dimer is strongest in stability, while the free G-quadruplex is weakest. Such a trend agrees qualitatively with the binding constant measurement in which L2H2-6OTD dimer (K_D = 8.3 nM) shows stronger binding than the monomer (K_D = 10.8 nM). Interestingly, ΔG_{unfold} is similar for different G-quartets incubated with the same ligand, which reflects the fact that ΔG_{unfold} is the state function independent of unfolding pathways.[15]

Quartet-by-Quartet Unfolding of G-Quadruplex Involves Two Energy Barriers. It is interesting that the difference in the rupture force between the G-quadruplex/telomestatin monomer and the G-quadruplex/telomestatin dimer complexes is more obvious from the unfolding via the middle G-quartet than those through terminal G-quartets (Figure 4). Such a difference can be rationalized by an unfolding model that involves two energy barriers (Figure 5).

The first (inner) barrier involves the unfolding of the G-quartet that is directly subject to mechanical stress. During the unfolding from the top or bottom G-quartet, due to the weaker contribution of the quartet stacking with respect to the loop interaction, the middle G-quartet is not as strong as the terminal quartets that interact more extensively with loops. As a result, the second (outer) barrier in these cases is dominated by the unfolding of the distally located terminal G-quartet (Figure 5, top and bottom panels, solid curves). Given that telomestatin dimer stacks to the two terminal quartets with similar strength, both the first and the second energy barriers increase their magnitudes to a similar level (Figure 5, top and bottom panels, green solid curves). On the other hand, due to the preferential binding of the telomestatin monomer to the top G-quartet,[8] only the top quartet increases the energy barrier. Therefore, during the unfolding from the top G-quartet, the first energy barrier (top quartet) is higher than the second (bottom quartet; see the blue solid curve in Figure 5, top panel), whereas this trend is reversed during the unfolding from the bottom G-quartet (see the blue solid curve in Figure 5, bottom panel) when monomer is bound.

During the unfolding through the middle G-quartet, the first energy barrier corresponds to the unfolding of the middle quartet, while the top and the bottom G-quartets represent the second barrier (Figure 5, middle). This geometry leads to a

Table 1. Change in Free Energy of Unfolding Telomeric G-Quadruplex [ΔG_{unfold} ± SD (bias), kcal/mol] with and without Telomestatin Derivatives

	no ligand	monomer	dimer
top	9.7 ± 0.4 (−0.4)	11 ± 4 (−0.3)	15 ± 2 (0.1)
middle	9.0 ± 0.6 (−0.5)	13 ± 2 (−0.3)	14 ± 2 (3.5)
bottom	9.9 ± 0.9 (1.4)	11 ± 2 (−0.1)	13 ± 2 (−0.3)

dx.doi.org/10.1021/ja503585h | J. Am. Chem. Soc. 2014, 136, 15537−15544

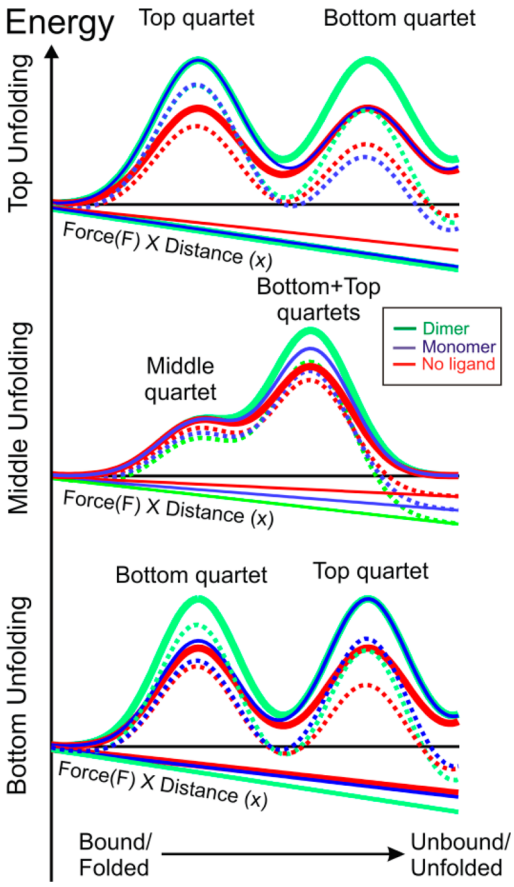

Figure 5. Proposed energetic diagram for the unfolding of G-quadruplex from the top, middle, or bottom G-quartet.

reduced distance between the two energy barriers. Because the terminal G-quartets are stronger than the middle quartet due to the loop interaction (see above), the second (outer) energy barrier is higher than the first (inner). Such an energy landscape renders the longest distance from the folded state to the highest energy barrier for the middle G-quadruplex among three G-quadruplexes (Figure 5). Since both top and bottom G-quartets bound with the dimer must be overcome before the whole G-quadruplex can be unfolded in this geometry, the second energy barrier in the presence of the telomestatin dimer is significantly higher than for the monomer, which binds to the top quartet only.

When force (F) is applied through a particular G-quartet, it reduces the free energy landscape with a magnitude of FX (solid lines in Figure 5; the slope of each line represents force F),[5] where X is the reaction coordinate of the unfolding. During the unfolding through the top or bottom G-quartet, due to the relatively large distance between the two energy barriers (ΔX), the outer energy barrier is more reduced than the inner barrier by $F\Delta X$. This leads to a predominant inner energy barrier after application of force (Figure 5, top and bottom panels, dotted curves). As a result, while unfolding through the top G-quartet, similar rupture forces exist between the telomestatin dimer and monomer, as both species stack to strengthen the top quartet, which is the inner barrier for this geometry. The difference in rupture forces becomes larger during the unfolding through the bottom G-quartet, since this quartet is the predominant inner barrier, which is strengthened by the telomestatin dimer but not the monomer.

In contrast, during the unfolding from the middle G-quartet, due to the much reduced distance between the two energy barriers, the outer energy barrier remains predominant, even after application of the force (Figure 5, middle panel; compare solid and dotted curves). Since the outer energy barrier represents both the top and bottom quartets in this geometry (see above), it leads to well-separated unfolding forces of the free G-quadruplex (weakest), the monomer-bound G-quadruplex, and the dimer-bound G-quadruplex (strongest). Finally, being the G-quadruplex with the longest distance (X) from the folded state to the highest energy barrier (see above and Figure 5), the unfolding force of the middle G-quadruplex is lowest among three G-quadruplexes due to the largest reduction of the energy barrier by a value of FX (see above). Such a prediction is well-validated by experimental observation in Figure 2b–d.

■ CONCLUSIONS

Using submolecular dissection of individual G-quartet planes in human telomeric DNA G-quadruplexes, we found that loop interaction contributes more to the G-quadruplex stability than the G-quartet stacking. These results suggest that in the design of ligands, molecules that interact with loops perhaps affect the structural stability more than those that intercalate with top or bottom G-quartet. As stacking modes of telomestatin derivatives can be well-differentiated at the submolecular level, we anticipate that this dissection method provides an alternative approach to probe ligand binding sites of biomacromolecules that are recalcitrant to conventional structural characterization methods.

■ ASSOCIATED CONTENT

Supporting Information

Figures S1–S3, illustrating the SPR determination of ligand binding with GQ, the G-quartet to phosphate distance, and CD data for ligand binding with GQ; Table S1, summarizing k_a, k_d, and K_D values of ligand binding with GQ; Table S2, outlining distance measurements for G-quartet to phosphate; and Table S3, compiling sequences of different unfolding geometries. This material is available free of charge via the Internet at http://pubs.acs.org.

■ AUTHOR INFORMATION

Corresponding Authors

knaga@cc.tuat.ac.jp
hs@kuchem.kyoto-u.ac.jp
hmao@kent.edu

Notes

The authors declare no competing financial interests.

■ ACKNOWLEDGMENTS

This research work was supported by NSF CHE-1026532 to H.M. It was supported in part by a Grant-in-Aid for Scientific Research (B) from JSPS (No. 23310158). K.N. is grateful for financial support from the Mukai Science and Technology Foundation, Tokyo, Japan, and Mochida Memorial Foundation for Medical and Pharmaceutical Research, Tokyo, Japan. K.I. is grateful for financial support in the form of JSPS Predoctoral Fellowships for Young Scientists. H.S. expresses sincere thanks for the CREST grant from the Japan Science and Technology Corporation (JST), grants from the WPI program (iCeMS, Kyoto University), and for the global COE program from the Ministry of Education, Culture, Sports, Science and Technol-

ogy (MEXT), Japan. We would also like to acknowledge Dr. Michael Zagorski and Colin Boyle from Case Western Reserve University for allowing us to use the CD instrument in their lab.

REFERENCES

(1) Biffi, G.; Tannahill, D.; McCafferty, J.; Balasubramanian, S. *Nat. Chem.* **2013**, *5*, 182.
(2) Hurley, L. H.; Wheelhouse, R. T.; Sun, D.; Kerwin, S. M.; Salazar, M.; Fedoroff, O. Y.; Han, F. X.; Han, H.; Izbicka, E.; Von Hoff, D. D. *Pharmacol. Ther.* **2000**, *85*, 141.
(3) Guittat, L.; Alberti, P.; Gomez, D.; De Cian, A.; Pennarun, G.; Lemarteleur, T.; Belmokhtar, C.; Paterski, R.; Morjani, H.; Trentesaux, C.; Mandine, E.; Boussin, F.; Mailliet, P.; Lacroix, L.; Riou, J. F.; Mergny, J. L. *Cytotechnology* **2004**, *45*, 75.
(4) Kim, M.-Y.; Vankayalapati, H.; Shin-ya, K.; Wierzba, K. a.; Hurley, L. H. *J. Am. Chem. Soc.* **2002**, *124*, 2098.
(5) Koirala, D.; Yangyuoru, P. M.; Mao, H. *Rev. Anal. Chem.* **2013**, *32*, 197.
(6) Williamson, J. R. *Annu. Rev. Biophys. Biomol. Struct.* **1994**, *23*, 703.
(7) Burge, S.; Parkinson, G. N.; Hazel, P.; Todd, A. K.; Neidle, S. *Nucleic Acids Res.* **2006**, *34*, 5402.
(8) Chung, W. J.; Heddi, B.; Tera, M.; Iida, K.; Nagasawa, K.; Phan, A. T. *J. Am. Chem. Soc.* **2013**, *135*, 13495.
(9) Guédin, A.; Gros, J.; Alberti, P.; Mergny, J. L. *Nucleic Acids Res.* **2010**, *38*, 7858.
(10) Fujimoto, T.; Nakano, S.-i.; Sugimoto, N.; Miyoshi, D. *J. Phys. Chem. B* **2012**, 963.
(11) Yu, Z.; Schonhoft, J. D.; Dhakal, S.; Bajracharya, R.; Hegde, R.; Basu, S.; Mao, H. *J. Am. Chem. Soc.* **2009**, *131*, 1876.
(12) Koirala, D.; Dhakal, S.; Ashbridge, B.; Sannohe, Y.; Rodriguez, R.; Sugiyama, H.; Balasubramanian, S.; Mao, H. *Nat. Chem.* **2011**, *3*, 782.
(13) Kolb, H. C.; Finn, M. G.; Sharpless, K. B. *Angew. Chem., Int. Ed.* **2001**, *40*, 2004.
(14) Krishna, H.; Caruthers, M. H. *J. Am. Chem. Soc.* **2012**, *134*, 11618.
(15) Yu, Z.; Koirala, D.; Cui, Y.; Easterling, L. F.; Zhao, Y.; Mao, H. *J. Am. Chem. Soc.* **2012**, *134*, 12338.
(16) Iida, K.; Majima, S.; Nakamura, T.; Seimiya, H.; Nagasawa, K. *Molecules* **2013**, *18*, 4328.
(17) Redman, J. E. *Methods* **2007**, *43*, 302.
(18) Rezler, E. M.; Seenisamy, J.; Bashyam, S.; Kim, M.-Y.; White, E.; Wilson, W. D.; Hurley, L. H. *J. Am. Chem. Soc.* **2005**, *127*, 9439.
(19) Wang, P.; Ren, L.; He, H.; Liang, F.; Zhou, X.; Tan, Z. *ChemBioChem* **2006**, *7*, 1155.
(20) Mao, H.; Luchette, P. *Sens. Actuators B* **2008**, *129*, 764.
(21) Baumann, C. G.; Smith, S. B.; Bloomfield, V. A.; Bustamante, C. *Proc. Natl. Acad. Sci. U.S.A.* **1997**, *94*, 6185.
(22) Dhakal, S.; Cui, Y.; Koirala, D.; Ghimire, C.; Kushwaha, S.; Yu, Z.; Yangyuoru, P. M.; Mao, H. *Nucleic Acids Res.* **2013**, *41*, 3915.
(23) Jarzynski, C. *Phys. Rev. Lett.* **1997**, *78*, 2690.
(24) Palassini, M.; Ritort, F. *Phys. Rev. Lett.* **2011**, *107*, 060601.
(25) Dai, J.; Punchihewa, C.; Ambrus, A.; Chen, D.; Jones, R. A.; Yang, D. *Nucleic Acids Res.* **2007**, *35*, 2440.
(26) Zhu, H.; Xiao, S.; Liang, H. *PLoS One* **2013**, *8*, e71380.
(27) Iida, K.; Tera, M.; Hirokawa, T.; Shin-ya, K.; Nagasawa, K. *Chem. Commun.* **2009**, 6481.
(28) Amemiya, Y.; Furunaga, Y.; Iida, K.; Tera, M.; Nagasawa, K.; Ikebukuro, K.; Nakamura, C. *Chem. Commun.* **2011**, *47*, 7485.